Biometric Identification of Mice

Kenneth Nilsson and Thorsteinn Rögnvaldsson
Halmstad University
School of Information Science, Computer and Electrical Engineering (IDE)
P.O. Box 823, SE-301 18 Halmstad, Sweden
Kenneth.Nilsson@ide.hh.se

Jens Cameron
DiLab, Scheelevägen 18, SE-223 63 Lund, Sweden

Christina Jacobson
AstraZeneca R&D, Scheelevägen 2, SE-221 87 Lund, Sweden

Abstract

We present a new application area for biometric recognition: the identification of laboratory animals to replace today's invasive methods. Through biometric identification a non invasive identification technique is applied with a code space that is restricted only by the uniqueness of the biometric identifier in use, and with an error rate that is predictable. In this work we present the blood vessel pattern in a mouse-ear as a suitable biometric identifier used for mouse identification. Genuine and Impostor score distributions are presented using a total of 50 mice. An EER of 2.5% is reported for images captured at the same instance of time which verifies the distinctive property of the biometric identifier.

1 Introduction

Identification of laboratory animals is essential in biomedical research. This is achieved by using, e.g., tattoos, freeze brands, subcutaneous electromagnetic transponders, ear notches and tags, or even toe-clipping (the latter is, however, considered inhumane) [5]. All these methods are to some degree invasive and restricted in code space (e.g. there is a limited number of notches that can be cut in a mouse's ear) and new methods are needed that are accurate, non-invasive (and humane) and with a larger code space.

Biometric identifiers, such as fingerprints, face geometry, voice, iris, retina etc. are today used to verify the identity of humans and it is natural to extend these ideas to animals, since animals also have individual physical characteristics. For instance, iris scans can be used for identifying horses [7] and retinal scans can be used for identifying cattle[1]. However, laboratory animals impose some specific requirements on the application; four out of five laboratory animals are rodents (e.g. mice and rats), which have small eyes and limbs, and the measurement must be quick and not unpleasant for the animal since the identification will be made several times, in connection with blood sampling, weighing, and so on. A retinal scan, which takes about 15 seconds to do on a cow, is completely unfeasible to do for each rodent in the lab several times a week.

We introduce in this paper a new biometric identifier, the blood vessel pattern in the ear, that can be measured very quickly on rodents and show that it may provide sufficient identification accuracy for use in biomedical research laboratories.

2 Blood Vessel Representation

We use a complex representation to model the spatial position and orientation of the blood vessels in the mouse-ear image. Each pixel is represented by a complex number

$$c(x,y) = \mu(x,y)e^{i\alpha(x,y)}. \quad (1)$$

where the magnitude $\mu(x,y)$ is a certainty measure for the existence of a blood vessel at the position (x,y) and the argument $\alpha(x,y)$ is the orientation of the vessel.

The left column of Figure 1 shows two gray scale mouse-ear images. The blood vessels appear as dark lines varying in width and orientation, which motivates using Gabor filters to extract them since Gabor filters are designed to be sensitive to specific frequency bands (scales) and to specific

[1] www.optibrand.com

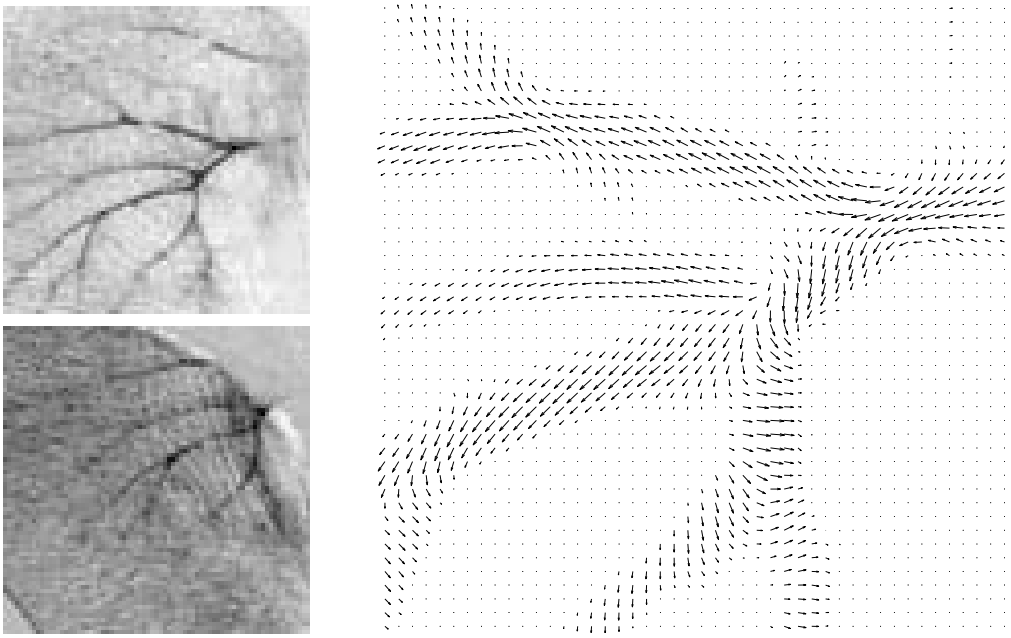

Figure 1. The two images to the left show gray scale mouse-ear images from the same mouse but taken on two different occasions. Blood-vessels appear as dark line-like structures of different widths and orientations. The right image shows the corresponding complex representation for the central part of the top image on the left side.

orientations of patterns [2]. The Gabor filter response is complex in the spatial domain; its real part, the cosine response, is sensitive to line patterns and its imaginary part, the sine response, is sensitive to edges in images. We use Gabor filters that are gaussian in the log-polar frequency domain [1, 6] to analyse the existence of blood vessels at different scales and orientations. Dark line-like structures, i.e. blood vessels, with different widths and orientations are enhanced in the gray scale image by computing a real valued dark-line response D according to

$$D(x, y, s, \theta) = -Re\{G\} - |Im\{G\}| \tag{2}$$

where $G = G(x, y, s, \theta)$ is the complex Gabor response in position (x, y), at scale s and for orientation θ. Re and Im are the real and imaginary operators, respectively. The $-Re\{G(x, y, s, \theta)\}$ part makes D sensitive to dark lines and the $-|Im\{G(x, y, s, \theta)\}|$ part lowers the response for edges.

Analysing the images at different scales $s_1, s_2, \ldots, s_K$ and orientations $\theta_1, \theta_2, \ldots, \theta_L$ increases the amount of data from $N \times M$ in the original gray scale image to $N \times M \times K \times L$ in the Gabor filtered image D. D is therefore synthesized to the final complex representation $c(x, y)$ of size $N \times M$ pixels by summing over the scales s_k and orientations θ_l:

$$c(x, y) = \sum_{l=1}^{L} |d(x, y, \theta_l)| \exp(i2\theta_l) \tag{3}$$

where

$$d(x, y, \theta_l) = \sum_{k=1}^{K} D(x, y, s_k, \theta_l). \tag{4}$$

The double angle representation is used to achieve a continuous representation, i.e. the orientation 0 should be close to the orientation π.

The right column of Figure 1 shows the complex representation for the central part of the top gray scale image in the left column. High certainty of blood vessels is coded by a large vector magnitude μ and the orientation of the vessel by the the direction of the vector, i.e. α.

3 Matching

Many data points, or distinctive features, should be used to achieve a robust matching result. As an example: the position and direction of unique feature points, called minutiae points (m-points), are often used when matching two fingerprints [4]. At least twelve m-points must match to secure the identification for human fingerprints [4].

For blood vessel patterns we define m-points as points where a blood vessel branches into two (or more). It is possible to identify 4 to 6 m-points in each image in Figure 1. The distinctiveness is high for m-points and their attributes: position and directions of branches are good features to use in the identification of mice. However, the m-points are few in numbers and therefore less suitable to use in isolation to match blood vessel pattern in a robust way. The number of m-points in a blood vessel pattern can be increased by also defining a point where the direction of a blood vessel is changing as an m-point.

Robust matching of blood vessel patterns, with many data points involved, is achieved by using the spatial position and the orientation of each pixel belonging to the blood-vessel pattern. The combination of many data points and unique feature points is also possible, i.e. to use position and local orientation of each pixel in the blood-vessel pattern together with its m-points as defined above.

The representation of the mouse-ear as a complex image gives us the possibility to identify each pixel in the blood vessel pattern and its m-points. A pixel belonging to the blood-vessel pattern is identified by a high magnitude μ and its orientation as the argument α of the complex number c. An m-point is identified by a change in the orientation around itself, i.e. a change of the argument of the complex number c in a neighborhood around a pixel.

Two images A and B are matched by computing a similarity measure between the two. This similarity measure is designed so that it gives a high score for similar images and a low score for dissimilar images. Each image is represented with complex numbers, i.e. the image A has pixel values $a(x,y) = \mu_A(x,y)\exp[i\alpha_A(x,y)]$ and the image B has pixel values $b(x,y) = \mu_B(x,y)\exp[i\alpha_B(x,y)]$. After the images have been properly aligned (registered) then the similarity measure is computed as

$$S = \frac{\sum_{x,y} Re\{a(x,y)\cdot b^*(x,y)\}}{\sqrt{\sum_{x,y}|a(x,y)|^2 \cdot \sum_{x,y}|b(x,y)|^2}}. \quad (5)$$

4 Experiments

4.1 Data

Two RGB-image databases, denoted *DB1* and *DB2*, were collected on two different occasions four months apart. Each database includes a total of 50 animals numbered as 1-50. Mice number 1-20 are the same individuals in the two databases. Five images per individual were taken for mice 1-20 in *DB1*. For all other mice in *DB1* and *DB2* is there only one image per individual.

The original images of high resolution were cropped manually to a size of 600×600 pixels to include most of the blood vessel pattern of the ear. Gray scale images were computed as the difference between the G and the R images to achieve a high contrast between background and blood vessels. The gray scale images were then down-sampled to 75×75 pixels before the Gabor filtering was done. The left column in Figure 1 shows examples of 75×75 gray scale images.

4.2 Blood Vessel Representation

The existence of blood vessels was analysed in the 75×75 gray scale images by Gabor filtering on three scales ($K = 3$) and for 18 orientation values ($L = 18$). The three scales covered blood vessel widths in the interval 3 to 8 pixels and the 18 orientation values covered the orientation interval $[0, \pi]$ uniformly.

4.3 Registration

We used pixel-by-pixel matching of aligned images, i.e. we first estimated the rotation and the translation parameters (there were no detectable scale differences between images) and compensated for the coordinate mismatch before matching. The rotation difference was estimated by using the algorithm presented by Li *et al.* [3] applied to the magnitude μ of the complex image. The translational difference was estimated by finding the position of the peak in the 2D cross-correlation function of the two rotationally aligned complex images. Compensation for the translational mismatch was then done and the pixels in the overlapping area of the two complex images were used for the matching.

4.4 Matching

A normalized similarity score, according to equation 5, was computed for the aligned complex images that should be matched. Only the complex pixel values in the common area of the two images were used for the score calculation.

Figure 2 shows the Genuine score distribution (at the top) and the Impostor score distribution (at the bottom) for images in *DB1*. The genuine score distribution is computed using mice 1-20. We have 5 images for each individual 1-20 (numbered as: a, b, c, d, and e) and 10 genuine scores are computed between images according to the scheme a-b, a-c, a-d, a-e ,b-c, b-d, b-e, c-d, c-e, and d-e, which gives a total of 200 scores (10×20). The impostor match is done by matching mice 21-50 to each of the mice 1-20 (only image number a), which yields a total of 600 scores (30×20). The resulting impostor score distribution is shown at the bottom of Figure 2.

The Equal Error Rate (EER) is 2.5% and is achieved for a threshold value of 0.65. This EER is of the same magnitude as those reported in fingerprint verification studies of FVC2000 and FVC2002 [4].

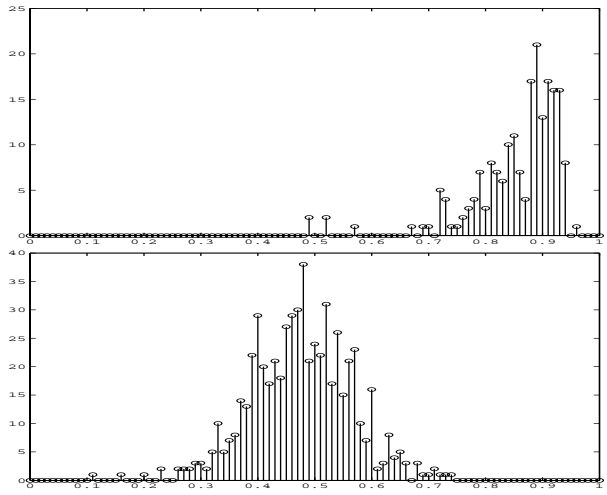

Figure 2. The top figure shows the Genuine score distribution for images in *DB1*. A total of 200 scores are computed from 20 mice and 5 images for each mouse. The Impostor scores for mice in *DB1* are shown in the bottom figure. A total of 600 scores are computed. The EER is 2.5%, which is achieved for a threshold value of 0.65.

A similar Genuine score distribution when matching mice 1-20 from the two databases *DB1* and *DB2* is shown in Figure 3. The two databases *DB1* and *DB2* were collected with a time difference of four months. Five computed scores for each individual gives a total of 95 scores (mouse 17 is missing from *DB2*).

Using the threshold value 0.65 yields a False Rejection Rate (FRR) of 11% , which is much higher than the FRR in *DB1*. However, when comparing manually the ear-images of mouse 13 in *DB2* and *DB1* it seems not to be the same individual. If mouse 13 in *DB2* is assumed to be erroneously labeled then the FRR shrinks to 6%. The higher FRR in *DB2*, compared to *DB1*, can at least partly be attributed to the higher degree of overlap between images within *DB1* than between *DB1* and *DB2*. This makes the estimation of the coordinate mismatch more difficult.

5 Conclusion

An EER of 2.5% is achieved for images captured at the same time (*DB1*). For images captured on two different occasions, four months apart, the FRR is increased to 6%. The higher error rate is not because of an unstable biometric identifier over time but due to a less than ideal degree of overlap between images from two occasions.

To conclude, the rodent ear blood vessel patterns are easy to capture and, as our experiments indicates, stable over time. It is possible to, already with a simple algorithm, use the blood vessel patterns to achieve identification error rates that are comparable to human fingerprints. Thus, the blood vessel pattern in mouse-ears can be considered as a very suitable biometric identifier for biometric non invasive laboratory mouse identification systems.

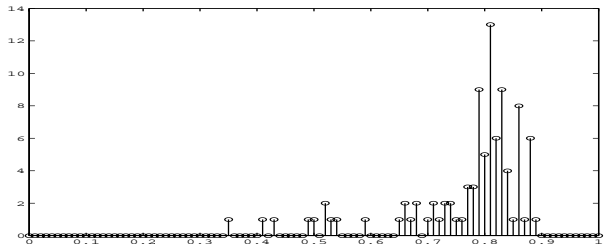

Figure 3. The Genuine score distribution between mice from *DB1* and *DB2*. A total of 95 scores are computed from 19 mice and 5 scores for each mice. A threshold value of 0.65 gives an FRR of 6% (when five scores lower then the threshold value are omitted because they are scores when comparing different individuals, i.e they should be low).

Acknowledgments

Supported by Vinnova and the Knowledge Foundation.

References

[1] J. Bigun. Speed, frequency, and orientation tuned 3-d gabor filter banks and their design. *In: Proc. Internat. Conf. on Pattern Recognition, ICPR, Jerusalem, IEEE Computer Society (1994)*, pages C–184–C–187, 1994.

[2] J. G. Daugman. Complete discrete 2-d gabor transforms by neural networks for image analysis and compression. *IEEE Trans. Acoustics, Speech, and Signal Processing*, 36:1169–1179, 1988.

[3] Z. Li, X. Yang, and L. Wu. Image registration based on hough transform and phase correlation. *IEEE Int. Conf. Neural Networks and Signal Processing*, December 2003.

[4] D. Maltoni, D. Maio, A. K. Jain, and S. Prabhakar. *Handbook of fingerprint recognition*. Springer, New York, 2003.

[5] C. on Rodents. *Rodents*. National Academy Press, Washington, D.C., 1996.

[6] F. Smeraldi. *Attention-driven pattern recognition*. Ph. d. thesis, Swiss Federal Institute of Technology, Lausanne, Switzerland (No. 2153 (200)), 2000.

[7] M. Suzaki, O. Yamakita, S. Orikawa, Y. Kuno, H. Aida, N. Sasaki, and R. Kusunose. A horse identification system using biometrics. *Systems and Computers in Japan*, 32:2686–2697, 2001.